HIPPOCAMPUS 25:159–168 (2015)

Excitation/Inhibition Imbalance and Impaired Synaptic Inhibition in Hippocampal Area CA3 of *Mecp2* Knockout Mice

Gaston Calfa, Wei Li, John M. Rutherford, and Lucas Pozzo-Miller*

ABSTRACT: Rett syndrome (RTT) is a neurodevelopment disorder associated with intellectual disabilities and caused by loss-of-function mutations in the gene encoding the transcriptional regulator Methyl-CpG-binding Protein-2 (MeCP2). Neuronal dysfunction and changes in cortical excitability occur in RTT individuals and *Mecp2*-deficient mice, including hippocampal network hyperactivity and higher frequency of spontaneous multiunit spikes in the CA3 cell body layer. Here, we describe impaired synaptic inhibition and an excitation/inhibition (E/I) imbalance in area CA3 of acute slices from symptomatic *Mecp2* knockout male mice (referred to as *Mecp2*$^{-/y}$). The amplitude of TTX-resistant miniature inhibitory postsynaptic currents (mIPSC) was smaller in CA3 pyramidal neurons of *Mecp2*$^{-/y}$ slices than in wildtype controls, while the amplitude of miniature excitatory postsynaptic currents (mEPSC) was significantly larger in *Mecp2*$^{-/y}$ neurons. Consistently, quantitative confocal immunohistochemistry revealed significantly lower intensity of the alpha-1 subunit of $GABA_A$Rs in the CA3 cell body layer of *Mecp2*$^{-/y}$ mice, while GluA1 puncta intensities were significantly higher in the CA3 dendritic layers of *Mecp2*$^{-/y}$ mice. In addition, the input/output (I/O) relationship of evoked IPSCs had a shallower slope in CA3 pyramidal neurons *Mecp2*$^{-/y}$ neurons. Consistent with the absence of neuronal degeneration in RTT and MeCP2-based mouse models, the density of parvalbumin- and somatostatin-expressing interneurons in area CA3 was not affected in *Mecp2*$^{-/y}$ mice. Furthermore, the intrinsic membrane properties of several interneuron subtypes in area CA3 were not affected by *Mecp2* loss. However, mEPSCs are smaller and less frequent in CA3 fast-spiking basket cells of *Mecp2*$^{-/y}$ mice, suggesting an impaired glutamatergic drive in this interneuron population. These results demonstrate that a loss-of-function mutation in *Mecp2* causes impaired E/I balance onto CA3 pyramidal neurons, leading to a hyperactive hippocampal network, likely contributing to limbic seizures in *Mecp2*$^{-/y}$ mice and RTT individuals.

KEY WORDS: Rett syndrome; MeCP2; Hippocampus; E/I balance; intellectual disability

INTRODUCTION

Partial and generalized convulsive or silent seizures occur in Rett syndrome (RTT), a neurodevelopmental disorder caused by mutations in *MECP2* (Amir et al., 1999). Consistent with the seizures observed in RTT individuals (Glaze et al., 1987; Steffenburg et al., 2001; Nissenkorn et al., 2010; Pintaudi et al., 2010; Cardoza et al., 2011), several lines of MeCP2-deficent mice exhibit seizure disorders (reviewed by Calfa et al., 2011b). Mice expressing a nonfunctional truncated protein (*Mecp2*^{308}) display repetitive generalized myoclonic jerks associated with high-amplitude bilateral cortical spikes and wave discharges in the electroencephalogram (EEG) (Shahbazian et al., 2002). *Mecp2* knockout mice also have seizure episodes with recurrent atypical EEG discharges in somatosensory cortex (Pelka et al., 2006; Chao et al., 2010; D'Cruz et al., 2010).

Electrophysiological recordings from principal neurons in slices from somatosensory cortex or thalamus, as well as from cultured hippocampal neurons from *Mecp2* knockout mice have shown reduced neuronal activity caused by a selective impairment in excitatory synaptic transmission (Dani et al., 2005; Nelson et al., 2006; Chao et al., 2007; Dani and Nelson, 2009; Noutel et al., 2011); but see (Nelson et al., 2011; Zhang et al., 2014), while a stronger innervation of pyramidal neurons by parvalbumin-expressing GABAergic interneurons causes a reduction in network activity in the visual cortex (Durand et al., 2012). On the other hand, neuronal activity in other brain regions is elevated, such as the hippocampus (Zhang et al., 2008; Calfa et al., 2011a) and brainstem (Kline et al., 2010). Using voltage-sensitive dye imaging, we demonstrated that hippocampal slices from male symptomatic *Mecp2* knockout mice (*Mecp2*$^{-/y}$) are hyperactive and more sensitive to epileptiform agents, which originates from a higher frequency of spontaneous spikes in CA3 pyramidal neurons (Calfa et al., 2011a). Here, we describe an imbalance of excitation/inhibition (E/I) inputs onto CA3 pyramidal neurons of symptomatic *Mecp2*$^{-/y}$ mice due to impaired synaptic inhibition, which drives the hyperactivity of the hippocampal network and likely contributes to atypical EEG and seizures disorders in MeCP2-deficient mice and RTT individuals.

Department of Neurobiology, Civitan International Research Center, The University of Alabama at Birmingham, Birmingham, Alabama

Additional Supporting Information may be found in the online version of this article.

Grant sponsor: NIH; Grant number: NS-065027, NS-40593; Grant sponsor: IRSF Postdoctoral Fellowships; Grant number: IRSF0804, IRSF2824.

Gaston Calfa is currently at IFEC-CONICET and Departamento de Farmacología, Facultad de Ciencias QuÚmicas, Universidad Nacional de Córdoba, Córdoba (5000), Argentina.

Gaston Calfa and Wei Li contributed equally to this work.

*Correspondence to: Lucas Pozzo-Miller, Department of Neurobiology, SHEL-1002, The University of Alabama at Birmingham, 1825 University Blvd., Birmingham, AL 35294-2182. E-mail: lucaspm@uab.edu

Accepted for publication 5 September 2014.

DOI 10.1002/hipo.22360

Published online 10 September 2014 in Wiley Online Library (wileyonlinelibrary.com).

MATERIAL AND METHODS

Animals

Female heterozygous *Mecp2* mice with deletions of exon 3 (*Mecp2*$^{tm1.1Jae}$ "Jaenisch line") (Chen et al., 2001) were obtained from the Mutant Mouse Regional Resource Center (University of California, Davis), and maintained in a pure C57/BL6 background by crossing them with wildtype C57/BL6 male mice. All experimental subjects were male hemizygous *Mecp2*$^{tm1.1Jae}$ knockout males (referred to as *Mecp2*$^{-/y}$) aged between postnatal days 40–60, when they exhibited RTT-like motor symptoms such as hypoactivity, hind limb clasping, and reflex impairments; age-matched wildtype male littermates were used as controls. Animals were handled and housed according to the Committee on Laboratory Animal Resources of the National Institutes of Health. All experimental protocols were reviewed and approved annually by the Institutional Animals Care and Use Committee of UAB.

Acute Hippocampal Slices

Mice were anesthetized with ketamine (100 mg/kg, i.p.) and transcardially perfused with ice-cold "cutting" artificial cerebrospinal fluid (aCSF) containing (m*M*): 110 choline-Cl, 26 glucose, 7 $MgCl_2$, 2.5 KCl, 1.25 NaH_2PO_4, 0.5 $CaCl_2$, 11.6 Na-ascorbate, 3 Na-pyruvate, 11 $NaHCO_3$, which was bubbled with 95% O_2/5% CO_2. Ventral hippocampal slices (300-μm-thick) were prepared using a vibratome (Leica VT1200S), and allowed to recover for at least 1 h at room temperature in a submerged chamber filled with aCSF containing (in m*M*): 129 NaCl, 3.5 KCl, 1.8 $MgSO_4$, 1.6 $CaCl_2$, 1.25 NaH_2PO_4, 26 $NaHCO_3$, 26 glucose; pH 7.4; saturated with 95% O_2/5% CO_2.

Whole-Cell Intracellular Recordings

Individual acute slices were transferred to a recording chamber mounted on a fixed-stage upright microscope (Leica DM-LFS, or Zeiss Axioskop-FS), and continuously perfused (2 mL/min) with aCSF at room temperature (24°C), containing (in m*M*): 121 NaCl, 5 KCl, 1.24 KH_2PO_4, 1.3 $MgSO_4$, 17.6 $NaHCO_3$, 2.5 $CaCl_2$, 10 glucose, and 29.2 sucrose (310–320 mOsm); aCSF was bubbled with 95% O_2 / 5% CO_2 (pH 7.4). Superficial pyramidal neurons in CA3 *stratum pyramidale* and interneurons within CA3 *stratum oriens* or *stratum lucidum* were visualized with a water-immersion 63X objective (0.9NA) using IR-DIC microscopy. Current-clamp experiments from pyramidal neurons were performed with unpolished whole-cell pipettes containing (in mM): 120 K-Gluconate, 17.5 KCl, 10 Na-HEPES, 4 Mg-ATP, 0.4 Na-GTP, 10 Na_2-creatine phosphate, 0.2 Na-EGTA; 290–300 mOsm; pH 7.3 (final resistance 3–4 MΩ), the aCSF contained CNQX (20 μM), APV (100 μM) and picrotoxin (50 μM). Voltage-clamp recordings from pyramidal neurons were performed with unpolished whole-cell pipettes containing (in mM): 120 Cs-gluconate, 17.5 CsCl, 10 Na-HEPES, 4 Mg-ATP, 0.4 Na-GTP, 10 Na_2-creatine phosphate, 0.2 Na-EGTA; 290–300 mOsm; pH 7.3 (final resistance 3–4 MΩ). Spontaneous mEPSCs in 1 μM TTX were recorded first at –60 mV, followed by recordings of mIPSCs at 0 mV in the same cells. Recordings of mEPSCs and spontaneous firing from interneurons were performed with unpolished whole-cell pipettes containing (in mM): 125 K-Gluconate, 10 KCl, 10 Na-HEPES, 2 Mg-ATP, 0.2 Na-GTP, 10 Na_2-creatine phosphate, 0.2 Na-EGTA; 290–300 mOsm; pH 7.3 (final resistance 3–4 MΩ). Recordings of mIPSC from interneurons were performed with pipettes containing (in mM): 137.5 KCl, 10 KCl, 10 Na-HEPES, 4 Mg-ATP, 0.4 Na-GTP, 10 Na_2-creatine phosphate, 0.2 Na-EGTA. Whole-cell pipettes for interneuron recordings also contained 2 mg/mL biocytin for post hoc morphological characterization. Slices were fixed in 4% paraformaldehyde in 100 mM phosphate buffer (PB), rinsed in PB saline (PBS, incubated with 1:250 Streptavidin Alexa-488, mounted on glass slides, and imaged by confocal microscopy (Olympus FV300, Argon laser, FITC filter, oil-immersion 60X 1.4NA objective).

Synaptic responses were evoked by stimulation of local interneurons within CA3 *stratum lucidum* and *stratum oriens* with 100μsec constant current pulses from a stimulus isolation unit (ISO-Flex, AMPI) connected to a patch electrode filled with oxygenated aCSF (final resistance 3–4 MΩ). IPSCs were evoked at 0 mV and isolated by using CNQX (20 μM) and APV (100 μM). Membrane currents and voltages were acquired with Axopatch-200B amplifiers (Molecular Devices), filtered at 2 kHz and digitized at 10 kHz with ITC-18 A/D-D/A interfaces (Instrutech) controlled by custom-written software in G5 PowerMac computers (TI-Work_Bench, provided by Dr. Takafumi Inoue). Spontaneous events were analyzed using MiniAnalysis (Synaptosoft).

Immunohistochemistry

Mice were anesthetized with ketamine and transcardially perfused with cold 4% paraformaldehyde in 100 mM PBS for 15 min. Brains were dissected by posterior craniotomy, placed in the above fixative at 4°C for 12 h, and cryoprotected by serial incubation in 15% and then 30% sucrose in 0.1 M PBS at 4°C (until sinking in every sucrose step). Brains were rinsed, dabbed dry, embedded in OCT (Tissue-Tek) and kept at −80°C. Brains were mounted and trimmed along the anterior–posterior axis to the vicinity of hippocampal formation using a Leica Jung CM3000 cryostat. Twenty-five micron coronal sections were cut and affixed to gelatin-subbed glass slides, which were kept at −20°C. Sections were allowed to warm to room temperature before rehydrating twice in 0.1 M PBS for 5 min; all following steps and solutions were at room temperature unless otherwise noted and performed with optimal volume on the glass slide by using a PAP pen (ImmEdge, Vector). Incubations longer than 10 min were performed in a humidified chamber.

For immunohistochemistry of GABAergic neurons, sections were permeabilized by incubation with 0.1% Triton-X 100 in

TABLE 1.

Kinetics of mIPSC and mEPSC Recorded from CA3 Pyramidal Neurons in Acute Slices from Wildtype and Mecp2$^{-/y}$ Mice

mIPSC	Wildtype (n=6 cells/5 mice)	*Mecp2*$^{-/y}$ (n=8 cells/7 mice)
Rise time (ms)	2.3 (2 − 2.8)	1.9 (1.8 − 2.5)
Decay time (ms)	13.5 (12.2 − 15.6)	13.8 (12.3 − 15.6)
mEPSC	**Wildtype (n=6 cells/5 mice)**	***Mecp2*$^{-/y}$ (n=6 cells/5 mice)**
Rise time (ms)	1.5 (1.2 − 2.1)	1.7 (1.5 − 2.6)
Decay time (ms)	6.6 (5.7 − 7.9)	8.4 (6.5 − 12.5)

Data are expressed as medians (quartiles in parentheses), and were compared with Mann Whitney test ($p > 0.05$).

0.1 M PBS (PBST) for 10 min. Antigen retrieval was performed by incubating sections twice with 10 mM sodium citrate, pH 3.0 with 0.05% Tween-20 for 10 min each, and then washing five times with PBST. Sections were blocked for 60 min with 10% normal goat serum (Sigma) in PBST followed by washing five times with PBST. Sections were incubated at 4°C for 16 h with 1:750 mouse anti-GAD67 (Millipore, MAB5406) and either 1:1,000 rabbit anti-parvalbumin (Abcam, ab11427) or 1:1670 rabbit antisomatostatin (Immunostar, 20089). After incubation slides were washed seven times with PBST prior to incubation for 2 h with 1:1,000 goat antimouse secondary antibody conjugated with AlexaFluor 568 and 1:1,000 goat antirabbit conjugated with AlexaFluor 488 (Invitrogen). Slides were washed seven times with PBS, covered with VectaShield (Vector), coverslipped, and stored at 4°C. Sections were imaged in a laser-scanning confocal microscope (Olympus FV300) using an oil-immersion 20 × 0.85 NA objective, and Argon and HeNe green lasers for excitation. Eight optical sections at 2.5-μm intervals were acquired from each fluorophore sequentially (FITC and TRITC emission filters; Semrock), and then displayed as maximum-intensity projections for cell counting (ImageJ; NIH). Four different cryostat sections through the hippocampus were imaged and analyzed per animal. Adjacent images were stitched together as needed using an ImageJ plugin (Preibisch et al., 2009). The CA3 region was defined as a wedge extending from the lateral tips of the dentate gyrus around to the point of inflection of *Cornu Ammonis*. Stacks of optical sections from each channel were analyzed separately from each other; positively stained cells were identified and counted per channel before blending; coincident positively stained cells were counted as positive for both antigens.

For immunohistochemistry of postsynaptic receptors containing either the GluA1 subunit of AMPA-type glutamate receptors, or the α-1 subunit of $GABA_A$ receptors, sections were permeabilized for 1 h with 0.25% Triton-X 100 in PBS, and blocked for 1 h with 10% normal serum. Sections were incubated at 4°C overnight with 1:200 rabbit anti-GluA1 (Millipore, AB1504) or anti- $GABA_A$ receptors α1 (Millipore, 06-868), followed by incubation with 1:300 antirabbit secondary antibody conjugated with AlexFluor 568 (Invitrogen). For the $GABA_A$ immunostaining, to visualize pyramidal cell nuclei sections were coincubated with mouse anti-NeuN (MAB377) and antimouse AlexFluor 488 secondary antibody (Invitrogen). Optical sections at 1 μm intervals were acquired with an oil-immersion 60 × 1.42 NA objective, and displayed for the CA3 region as described above. Laser power and photomultiplier gain were set at the same levels for all sections imaged to allow quantitative comparisons of immunolabeling intensities of between wildtype and *Mecp2* knockout sections. The number of puncta within each layer of area CA3, *stratum oriens* (SO), *stratum pyramidale* (SP), *stratum lucidum* (SL), and *stratum radiatum* (SR), was counted with a particle analysis plug-in of ImageJ using a defined puncta size range.

Statistical Analyses

For all quantitative analyses, the experimenters were blind to the genotype. All data are shown as the mean ± S.E.M, and compared by parametric unpaired Student's *t*-test, or nonparametric Mann-Whitney, or Kolmogorov-Smirnov tests using Prism (GraphPad) and MiniAnalysis programs. Differences between group means were considered significant at $P < 0.05$.

RESULTS AND DISCUSSION

Voltage-sensitive dye imaging revealed that hippocampal slices from symptomatic *Mecp2* male knockout mice (*Mecp2*$^{-/y}$) are hyperactive, and more sensitive to the epileptiform agent 4-AP (Calfa et al., 2011a). Network hyperactivity originated from area CA3, which showed a higher frequency of spontaneous multiunit spikes (Calfa et al., 2011a). To find the cellular origin of such network hyperactivity, we first characterized the intrinsic membrane properties of CA3 pyramidal neurons under current-clamp and in the absence of excitatory and inhibitory inputs (DL-APV, CNQX, and picrotoxin). All intrinsic membrane properties were comparable in CA3 pyramidal neurons from both genotypes (Supporting Information Table 1; $P > 0.05$). Intrinsic excitability was estimated by the number of spikes fired at different amplitudes of direct current injection (Supporting Information Fig. 1A). The fitted slopes (m) of the linear portion of such firing-input (F-I) curves (Supporting Information Fig. 1B) were similar in wildtype (0.12 ± 0.02, n = 5 cells/3 mice) and *Mecp2*$^{-/y}$ mice (0.17 ± 0.02, n = 6/3; P = 0.124). Also, the amplitudes of the fast afterhyperpolarization (fAHP; Supporting Information Fig. 1C), and the slow AHP (sAHP; Supporting Information Fig. 1D) were similar in both genotypes ($P > 0.05$). Consistent with an earlier study in the Bird line of *Mecp2* knockout mice (Zhang et al., 2008), these data indicate that the intrinsic excitability of CA3 pyramidal

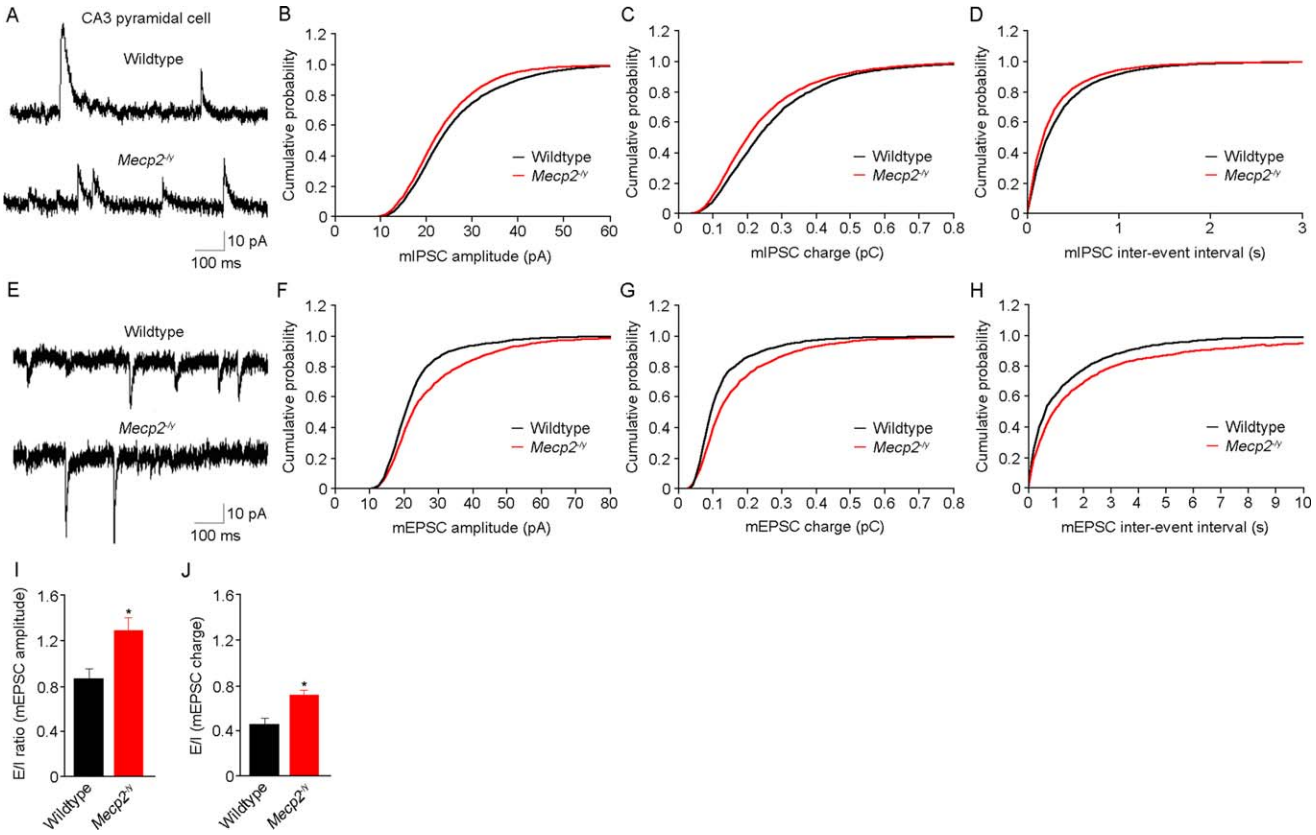

FIGURE 1. Spontaneous quantal synaptic transmission onto CA3 pyramidal neurons. A: Representative examples of mIPSCs. B: The cumulative probability distribution of mIPSC amplitudes recorded in *Mecp2*$^{-/y}$ CA3 pyramidal neurons was shifted toward the left compared to wildtype neurons. C: The cumulative probability distribution of mIPSC charges in *Mecp2*$^{-/y}$ CA3 pyramidal neurons was shifted toward the left compared with wildtype neurons. D: The cumulative probability distribution of mIPSC interevent intervals in *Mecp2*$^{-/y}$ CA3 pyramidal neurons was shifted toward the left compared with wildtype neurons, i.e., higher mIPSC frequency. E: Representative examples of mEPSCs. F: The cumulative probability distribution of mEPSC amplitudes recorded in *Mecp2*$^{-/y}$ CA3 pyramidal neurons was shifted toward the right compared to wildtype neurons. G: The cumulative probability distribution of mEPSC charge in *Mecp2*$^{-/y}$ CA3 pyramidal neurons was shifted toward the right compared to wildtype neurons. H: The cumulative probability distribution of mEPSC inter-event intervals in *Mecp2*$^{-/y}$ CA3 pyramidal neurons was shifted toward the right compared to wildtype neurons, i.e., lower mEPSC frequency. I: The ratio of the amplitudes of mEPSCs to mIPSCs in CA3 pyramidal neurons is higher in *Mecp2*$^{-/y}$ mice compared to wildtype mice. These mEPSCs and mIPSCs where obtained from the same cells at different holding potentials. J: The ratio of the charges of mEPSCs to mIPSCs in CA3 pyramidal neurons is higher in *Mecp2*$^{-/y}$ mice compared with wildtype mice; same cells as in I. [Color figure can be viewed in the online issue, which is available at wileyonlinelibrary.com.]

neurons is not affected by *Mecp2* deletion, and thus should not contribute to hippocampal network hyperactivity.

Next, we recorded TTX-resistant miniature inhibitory and excitatory postsynaptic currents (mIPSC and mEPSC, respectively; 1 μM TTX) to evaluate spontaneous quantal synaptic input onto CA3 pyramidal neurons (Figs. 1A,E). The cumulative probability distribution of mIPSC amplitude and charge recorded in *Mecp2*$^{-/y}$ CA3 pyramidal neurons (n = 8 cells/7 mice) was shifted toward the left compared to wildtype neurons (n = 6/5; $P < 0.001$, Kolmogorov-Smirnov test: KS-Z value = 5.3 for mIPSC amplitude; KS-Z value = 7.59 for mIPSC charge) (Figs. 1B,C). Intriguingly, the cumulative probability distribution of mIPSC interevent intervals in *Mecp2*$^{-/y}$ CA3 pyramidal neurons was shifted toward the left compared to wildtype neurons, i.e., higher mIPSC frequency ($P < 0.001$, KS-Z value = 6.6) (Fig. 1D). On the other hand, the cumulative probability distribution of mEPSC amplitude and charge recorded in *Mecp2*$^{-/y}$ CA3 pyramidal neurons (n = 6 cells/5 mice) was shifted toward the right compared to wildtype neurons (n = 6 /5; $P < 0.001$; KS-Z value = 4.4 for mEPSC amplitude; KS-Z value = 5.8 for mEPSC charge) (Figs. 1F,G). The cumulative probability distribution of mEPSC interevent intervals in *Mecp2*$^{-/y}$ CA3 pyramidal neurons was shifted toward the right compared to wildtype neurons, i.e., a lower mEPSC frequency (P = 0.0001; KS-Z value = 2.2) (Fig. 1H). No significant changes were observed in the kinetics of individual mEPSCs and mIPSCs between wildtype and *Mecp2*$^{-/y}$ neurons (Table 1; $P > 0.05$ Mann Whitney test).

Calculating the ratio of mEPSC and mIPSC amplitudes recorded from the same CA3 pyramidal neurons at different

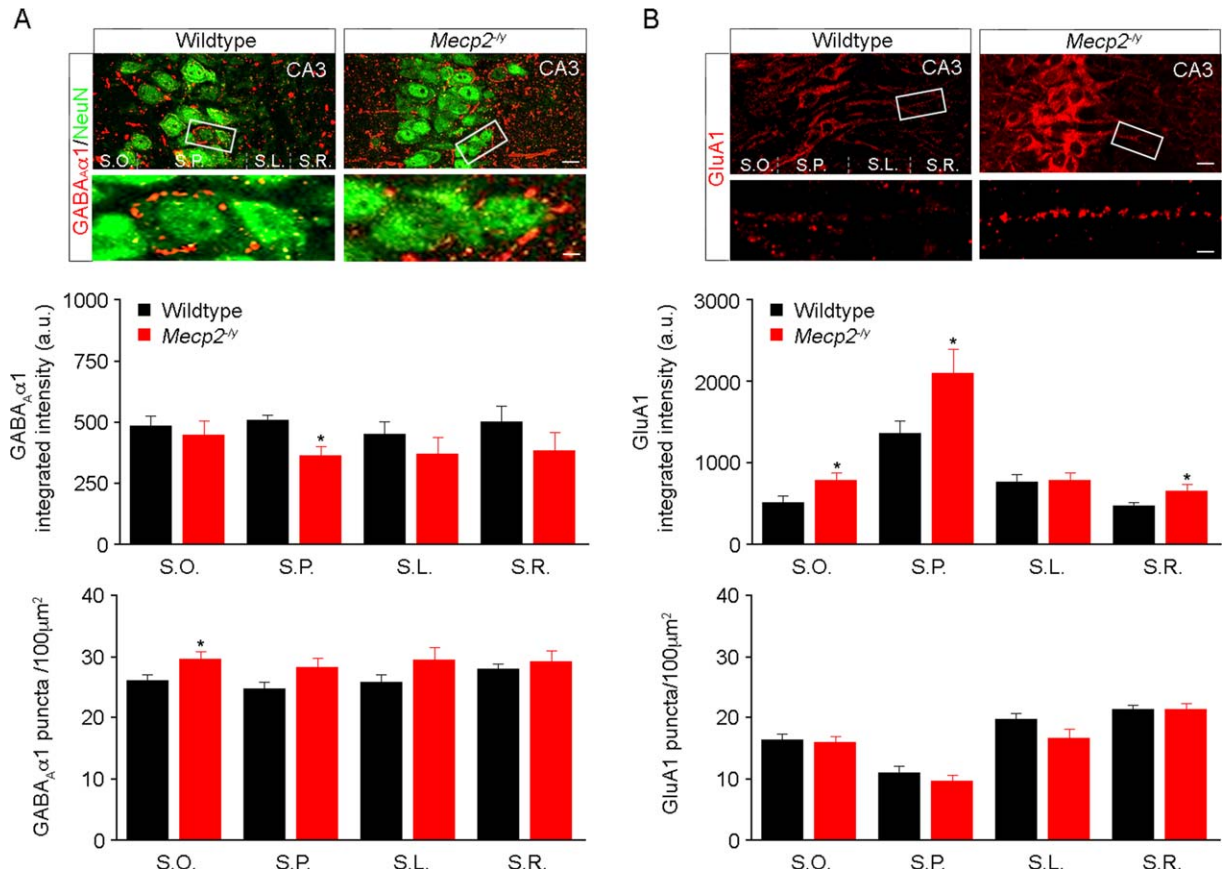

FIGURE 2. Inhibitory and excitatory postsynaptic puncta in area CA3. A, top: Representative confocal microscopy images of dual immunolabeling of $GABA_A\alpha1$ and the neuronal nuclear marker NeuN in area CA3 of wildtype (left) and *Mecp2*$^{-/y}$ mice (right). Region inside white box is enlarged at the bottom, and shows postsynaptic $GABA_AR$ clusters around CA3 pyramidal neurons. Bottom, Quantification of the pixel intensity and numerical density of $GABA_A\alpha1$ immunopositive puncta in the different layers of area CA3 (S.O. *stratum oriens*; S.P. *stratum pyramidale*; S.L. *stratum lucidum*; S.R. *stratum radiatum*). B top, Representative confocal microscopy images of immunolabeling of GluA1 in area CA3 of wildtype (left) and *Mecp2*$^{-/y}$ mice (right). Region inside white box is enlarged at the bottom, and shows postsynaptic AMPAR clusters in the dendritic regions of CA3. Scale bars are 50 μm (top) and 10 μm (insets). Bottom, Quantification of the pixel intensity and numerical density of GluA1 immunopositive puncta in the different layers of area CA3; asterisks denote $P < 005$. [Color figure can be viewed in the online issue, which is available at wileyonlinelibrary.com.]

holding potentials (−65 mV for mEPSCs, 0 mV for mIPSCs) yielded a larger E/I ratio in *Mecp2*$^{-/y}$ neurons (1.25 ± 0.3; n = 6 cells/5 mice) compared to wildtype neurons (0.8 ± 0.1; n = 6/5; P = 0.039) (Fig. 1I). Similarly, the ratio of mEPSC charge to mIPSC charge obtained from the same CA3 pyramidal neurons is higher in *Mecp2*$^{-/y}$ neurons (0.7 ± 0.1) compared to wildtype ones (0.5 ± 0.1; P = 0.0036) (Fig. 1J). This analysis demonstrates an imbalance in the excitation-to-inhibition ratio of spontaneous quantal synaptic transmission arriving onto CA3 pyramidal neurons.

We next performed quantitative analyses of confocal immunohistochemical staining of postsynaptic receptors at inhibitory and excitatory hippocampal synapses. For inhibitory synapses, we chose the α-1 subunit of $GABA_ARs$ because it is expressed in area CA3 (Hortnagl et al., 2013) in a punctate pattern in principal cells (Frola et al., 2013). The pixel intensity of fluorescent puncta immunopositive for the α-1 subunit of $GABA_ARs$ was significantly lower in the CA3 pyramidal cell body layer of *Mecp2*$^{-/y}$ mice (*stratum pyramidale*; 357.9 ± 38.9; n = 15; P = 0.005), while their numerical density was significantly higher on their basal dendrites in *stratum oriens* (30 ± 1.3; n = 14; P = 0.046; Fig. 2A). These observations are consistent with the higher frequency of smaller mIPSCs recorded from *Mecp2*$^{-/y}$ CA3 pyramidal neurons (Fig. 1), which originate from proximal presynaptic terminals. Furthermore, the pixel intensity of GluA1 puncta was significantly higher in the distal apical dendrites of *stratum radiatum* (652.1 ± 75.9; n = 10; P = 0.036), the basal dendrites in *stratum oriens* (781.5 ± 93.9; n = 9; P = 0.029), and the cell body layer (2113 ± 296.4; n = 11; P = 0.026) of *Mecp2*$^{-/y}$ mice (Fig. 2B), which is consistent with larger mEPSCs, which mainly originate from distal presynaptic terminals (Lawrence and McBain, 2003). On the other hand, differences in the numerical density of GluA1 puncta did not reach statistical significance in any of the CA3 layers (P > 0.05; Fig. 2B).

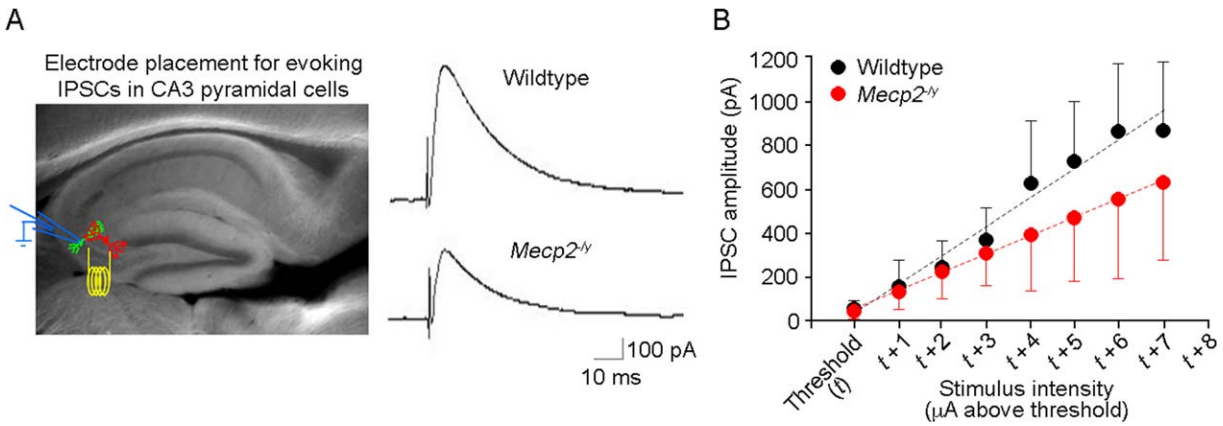

FIGURE 3. Evoked synaptic inhibition onto CA3 pyramidal neurons. A, Electrode placement and representative examples of IPSCs evoked in CA3 pyramidal neurons clamped at 0 mV by stimulation of local interneurons within CA3 *stratum lucidum* in the presence of APV/CNQX. B: Input-Output (I-O) relationship between the amplitude of evoked IPSCs and stimulation intensity. The fitted slope (m) of the linear portion of the I-O curve was significantly smaller in *Mecp2*$^{-/y}$ slices than in wildtype slices. [Color figure can be viewed in the online issue, which is available at wileyonlinelibrary.com.]

To determine whether action potential-driven synaptic inhibition was also affected by *Mecp2* deletion, we evoked IPSCs in CA3 pyramidal neurons clamped at 0 mV by stimulating local interneurons in CA3 *stratum lucidum* in the presence of APV and CNQX (Fig. 3A). The fitted slope (m) of the linear portion of input-output (I-O) relationships of evoked IPSCs was significantly smaller in

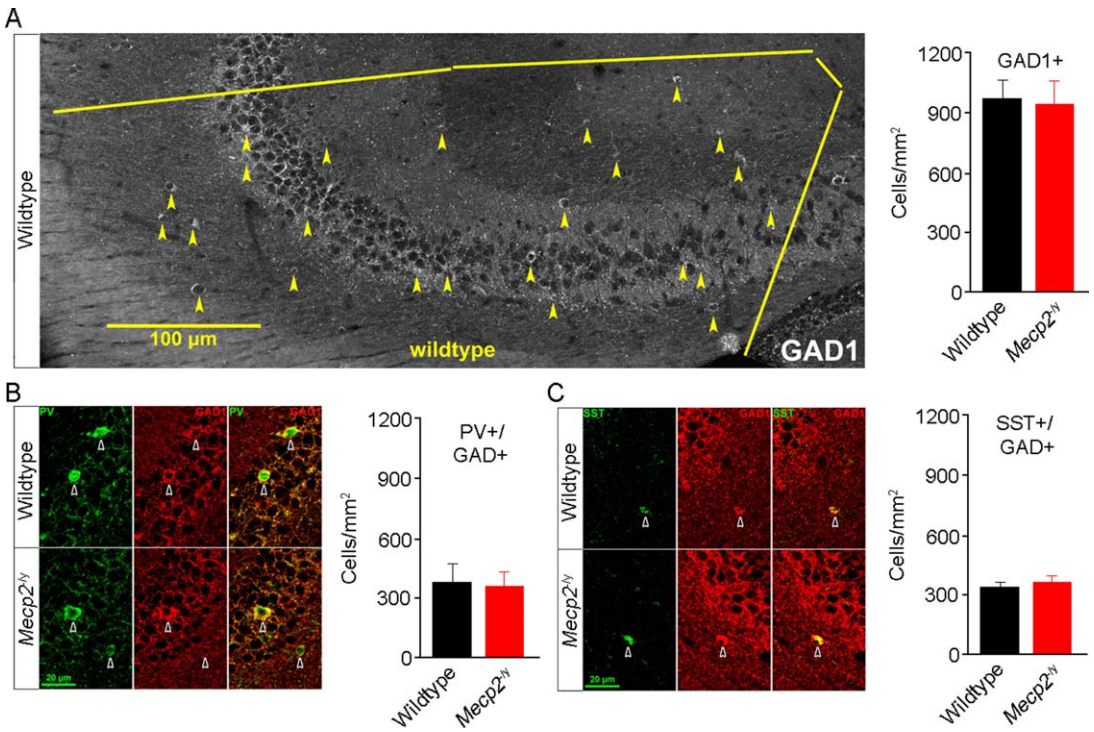

FIGURE 4. Interneuron cell density in area CA3. A left, Representative example of a wildtype brain section including the hippocampus, which was immunostained with anti-GAD1 antibodies to illustrate the region used for quantitative analyses of interneuron cell density (confocal microscopy). Lines enclose the region analyzed for cell density: the wedge of dorsal hippocampus from the tips of the dentate gyrus laterally to the point of inflection of *Cornu Ammonis*. Arrowheads point to GAD1 immunopositive cells. Right, number of GAD1 positive cells per mm^2 of area CA3. B left, Representative examples of PV and GAD1 double immunostaining in area CA3 of wildtype (top) and Mecp2$^{-/y}$ (bottom) mice. Arrowheads point to PV/GAD1 double-positive cells. Right, number of PV/GAD1 double-positive positive cells per mm^2 of area CA3. C left, Representative examples of SST and GAD1 immunostaining in area CA3 of wildtype (top) and Mecp2$^{-/y}$ (bottom) mice. Arrowheads point to SST/GAD1 double-positive cells. Right, number of SST/GAD1 double-positive positive cells per mm^2 of area CA3. [Color figure can be viewed in the online issue, which is available at wileyonlinelibrary.com.]

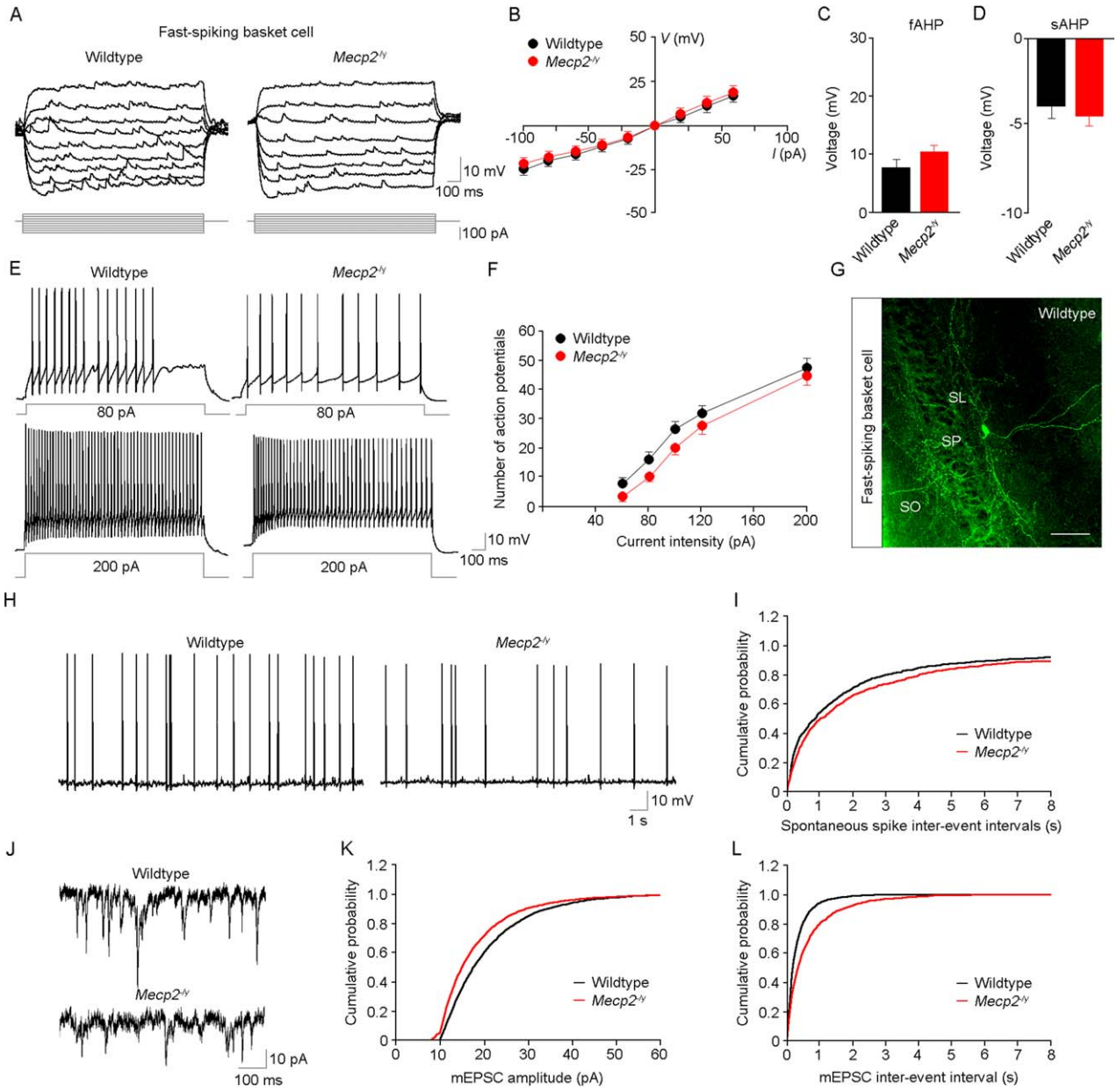

FIGURE 5. Intrinsic and synaptic properties of CA3 fast-spiking basket interneurons. A: Representative subthreshold voltage responses in CA3 fast-spiking basket cells of wildtype (left) and *Mecp2*$^{-/y}$ mice (*right*). Current injections from −100 to 60 pA in 20 pA increments. B: I-O relationship between current intensity and subthreshold voltage responses. No significant differences were observed between wildtype (n = 24 cells/14 mice) and *Mecp2*$^{-/y}$ interneurons (n = 29 cells/20 mice). C,D: The amplitudes of the fAHP (C) and sAHP (D) were similar between two genotypes. E: Representative firing responses of fast-spiking basket cells from wildtype (left) and *Mecp2*$^{-/y}$ mice (right) evoked by 80pA (top) and 200pA (bottom) current injections. F: I-O relationship between current intensity and the number of action potentials. Two-way repeated ANOVA analysis shows significant differences between two genotypes (P = 0.003); post hoc comparisons indicate tendency to significance for fewer spikes in *Mecp2*$^{-/y}$ mice for the low current injection groups (60 pA, P = 0.068; 80 pA, P = 0.079; 100 pA, P = 0.078). G: Representative example of a wildtype fast-spiking basket cell filled with biocytin, stained with Alexa-488-conjugated streptavidin, and imaged by confocal microscopy; scale bar = 100 μm. H: Representative examples of spontaneous firing recorded in CA3 fast-spiking basket cells. I: Cumulative probability distribution of spontaneous firing in *Mecp2* knockout interneurons was shifted toward the right (wildtype n = 14 cells/8 mice, *Mecp2*$^{-/y}$ n = 23 cells/11 mice; K-S test P < 0.001). J: Representative examples of mEPSCs in CA3 fast-spiking basket cells of wildtype (top) and *Mecp2*$^{-/y}$ mice (bottom). K,L: Cumulative probability distribution of mEPSC amplitude (K) in *Mecp2* knockout interneurons was shifted toward the left (wildtype n = 7 cells/6 mice, *Mecp2*$^{-/y}$ n = 13 cells/8 mice; K-S test P < 0.001), and that of mEPSC inter-event intervals (*L*) toward the right (K-S test P < 0.001). [Color figure can be viewed in the online issue, which is available at wileyonlinelibrary.com.]

TABLE 2.

Intrinsic Properties of Different CA3 Interneuron Types in Acute Slices from Wildtype and **Mecp2^{-y}** *Mice*

Fast-spiking basket cells	Wildtype (n=24 cells/15 mice)	*Mecp2*$^{-y}$ (n=29 cells/16 mice)
Resting potential (mV)	−46.5 ± 0.7	−44.7 ± 0.7
Delay to first spike (ms)	7.3 ± 0.6	6.9 ± 0.5
Spike threshold (mV)	−34.7 ± 3.1	−32.1 ± 3.7
Spike amplitude (mV)	77.2 ± 2.1	71.9 ± 1.8
Spike width at half amplitude (ms)	1.00 ± 0.04	1.05 ± 0.03
Accommodation ratio	1.87 ± 0.13	1.87 ± 0.12
Regular-spiking basket cells	Wildtype (n=9 cells/7 mice)	*Mecp2*$^{-/y}$ (n=9 cells/9 mice)
Resting potential (mV)	−45.1 ± 0.9	−44.4 ± 1.5
Delay to first spike (ms)	5.8 ± 0.9	5.4 ± 0.5
Spike threshold (mV)	−38.1 ± 1.1	−38.5 ± 1.5
Spike amplitude (mV)	73.1 ± 4.2	67.8 ± 2.7
Spike width at half amplitude (ms)	1.27 ± 0.06	1.33 ± 0.03
Accommodation ratio	2.39 ± 0.21	2.67 ± 0.31
Spiny lucidum cells	Wildtype (n=5 cells/5 mice)	*Mecp2*$^{-y}$ (n=6 cells/4 mice)
Resting potential (mV)	−46.2 ± 1.6	−47.5 ± 1.7
Delay to first spike (ms)	8.9 ± 1.2	9.1 ± 1.4
Spike threshold (mV)	−38.3 ± 1.2	−40.6 ± 1.6
Spike amplitude (mV)	70.3 ± 6.4	73.9 ± 7.2
Spike width at half amplitude (ms)	1.19 ± 0.11	1.15 ± 0.09
Accommodation ratio	2.61 ± 0.34	2.27 ± 0.23
Mossy fiber-associated cell	Wildtype (n=7 cells/7 mice)	*Mecp2*$^{-y}$ (n=6 cells/5 mice)
Resting potential (mV)	−44.7 ± 0.9	−46.3 ± 0.8
Delay to first spike (ms)	7.8 ± 1.1	6.7 ± 0.6
Spike threshold (mV)	−38.8 ± 1.5	−40.7 ± 1.1
Spike amplitude (mV)	59.3 ± 5.5	65.1 ± 3.4
Spike width at half amplitude (ms)	1.42 ± 0.11	1.43 ± 0.19
Accommodation ratio	2.41 ± 0.19	2.72 ± 0.11

Data were analyzed with Mann Whitney test (p>0.05).

Mecp2$^{-/y}$ slices (m = 79 ± 7; n = 16 cells/8 mice; R^2 = 0.99) than in wildtype slices (m = 133 ± 15; n = 13/7; R^2 = 0.97; P = 0.0018) (Fig. 3B), indicating weaker inhibitory synaptic transmission onto *Mecp2*$^{-/y}$ CA3 pyramidal neurons.

To begin searching the causes of impaired inhibitory synaptic transmission, we first performed a quantitative analysis of interneuron cell density in area CA3 by immunohistochemistry. The density of glutamic acid decarboxylase 1 (GAD1) positive interneurons was comparable in area CA3 of both genotypes (wildtype 971.1 ± 85.0, n = 3 *vs.* *Mecp2*$^{-/y}$ 946.3 ± 111.6, n = 4; P = 0.8752; Fig. 4A). Similarly, the density of parvalbumin (PV) and GAD1 double-positive interneurons, which mostly target the somata of CA3 pyramidal neurons as basket cells, was not affected by *Mecp2* deletion (wildtype 387.8 ± 94.9 *vs.* *Mecp2*$^{-/y}$ 373.0 ± 70.5, n = 3; P = 0.9065; Fig. 4B). Also, the density of somatostatin (SOM) and GAD1 double-positive interneurons, which target more distal dendritic regions of CA3 pyramidal neurons, was comparable in mice from both genotypes (wildtype 309.0 ± 21.1 vs. *Mecp2*$^{-/y}$ 344.2 ± 30.9, n = 3; P = 0.3993; Fig. 4C).

Next, we performed whole-cell recordings from 4 different subtypes of interneurons present in area CA3 identifying them by their intrinsic firing properties (Supporting Information Fig. 2), location, and morphology: fast-spiking basket cells, regular-spiking basket cells, spiny lucidum cells, and mossy fiber-associated cells (Szabadics and Soltesz, 2009). All intrinsic membrane properties were comparable in all these interneuron types from both genotypes (Table 2; $P > 0.05$; Figs. 5A–F for fast-spiking basket cells; Supporting Information Fig. 3 for regular-spiking basket cells; Supporting Information Fig. 4 for spiny lucidum cells; Supporting Information Fig. 5 for mossy fiber-associated cells). Notably, the frequency of spontaneous action potentials in fast-spiking basket cells was significantly smaller in *Mecp2*$^{-/y}$ mice compared with wildtype littermates (wildtype n = 14 cells/8 mice, *Mecp2*$^{-/y}$ n =2 3/11; K-S test $P < 0.001$; Figs. 5H,I). Analyses of asynchronous transmitter release onto CA3 interneurons revealed that fast-spiking basket cells received smaller mEPSCs with a slower frequency in *Mecp2*$^{-/y}$ knockouts than in wildtype mice (wildtype n = 7/6 vs. *Mecp2*$^{-/y}$ n = 13 cells/8 mice; K-S test $P < 0.001$; Figs.

5J–L). These results suggest that asynchronous excitatory drive onto one of the most critical interneuron types in CA3 is weaker in *Mecp2*$^{-/y}$ knockouts.

The consequences of MeCP2 dysfunction on neuronal network function, as well as on synaptic function and plasticity vary in different brain regions ought to specific time courses and sequences of excitatory and inhibitory synapse formation in each area (Shepherd and Katz, 2011; Kron et al., 2012). For example, principal neurons in slices from somatosensory cortex or thalamus from *Mecp2* knockout mice have reduced neuronal activity caused by a selective impairment in excitatory synaptic transmission, as well as by hypo-connectivity between excitatory neurons (Dani et al., 2005; Dani and Nelson, 2009; Noutel et al., 2011; but see Nelson et al., 2011; Zhang et al., 2014). Intriguingly, the visual cortex of *Mecp2* knockout mice shows a similar reduction of pyramidal neuron and network activity, but due to stronger inhibition from a hyperinnervation by parvalbumin-expressing interneurons (Durand et al., 2012). In addition, a recent report demonstrated that deletion of *Mecp2* specifically in excitatory neurons caused impaired GABAergic transmission onto cortical pyramidal neurons, which led to seizures and cortical hyperexcitation (Zhang et al., 2014). Neuronal activity in other brain regions of *Mecp2* knockout mice is elevated, such as the hippocampus (Zhang et al., 2008; Calfa et al., 2011a) and brainstem (Kline et al., 2010). Consistent with our results and those in mice with selective *Mecp2* deletion in excitatory neurons (Zhang et al., 2014), impaired GABAergic inhibition was also described in the thalamus (Zhang et al., 2010) and brainstem (Medrihan et al., 2008), and it involved a reduction in the number of GABAergic synapses onto principal neurons. Indeed, selective deletion of *Mecp2* in GABAergic neurons led to impaired GABAergic transmission, cortical hyperexcitability and several neurological features of RTT and autism spectrum disorders (Chao et al., 2010).

An unbalance of the excitation-to-inhibition ratio has emerged as common feature in several neurodevelopmental disorders, including autism-spectrum disorders, Tourette syndrome and Down syndrome (Rubenstein and Merzenich, 2003; Di Cristo, 2007). Of relevance to the intellectual disability associated to RTT, the cognitive deficits observed in mouse models of Down syndrome (Ts65Dn) (Kleschevnikov et al., 2004), neurofibromatosis (Costa et al., 2002; Li et al., 2005) and Fragile X (Gibson et al., 2008) are caused by an excitatory/inhibitory imbalance of synaptic function in the hippocampus. Of relevance to potential therapeutic approaches, these impairments can be reverted by pharmacological manipulations in adult symptomatic animals (Costa et al., 2002; Li et al., 2005; Fernandez et al., 2007; Rueda et al., 2008); reviewed by (Ehninger et al., 2008).

Since MeCP2 controls *Bdnf* expression (reviewed by Li and Pozzo-Miller, 2014), and BDNF modulates the development of GABAergic neurons and synapses (reviewed by Vicario-Abejon et al., 2002), all the above observations suggest that impaired BDNF signaling in *Mecp2*-deficient brains is unable to support proper GABAergic synapse formation and maturation. In fact, deletion of *Bdnf* in individual neurons results in reduced GABAergic innervation on each neuron lacking BDNF (Kohara et al., 2007). Notably, increasing BDNF levels or its TrkB-mediated signaling improves neurological symptoms in *Mecp2* deficient mice (Chang et al., 2006; Ogier et al., 2007; Kline et al., 2010; Schmid et al., 2012). Taken together, these results indicate that the balance of synaptic inhibition is weakened in area CA3, a situation that favors runaway excitation of the highly interconnected network of CA3 pyramidal neurons and leads to hippocampal hyperactivity and limbic seizures in *Mecp2*$^{-/y}$ mice and RTT individuals.

ACKNOWLEDGMENTS

The authors thank Ms. Lili Mao for mouse colony management, Dr. Xin Xu for comments on the manuscript, and Dr. Takafumi Inoue (Waseda University, Tokyo, Japan) for data acquisition and analysis software. They are thankful for pilot immunohistochemistry imaging of presynaptic puncta performed by Dr. Jennifer Larimore (Agnes Scott College, Decatur, GA). The Alabama Neuroscience Blueprint Core Center (NS-57098), the UAB Intellectual and Developmental Disabilities Research Center (HD-38985), and the UAB Neuroscience Core (NS-47466) provided instrumentation.

REFERENCES

Amir RE, Van den Veyver IB, Wan M, Tran CQ, Francke U, Zoghbi HY. 1999. Rett syndrome is caused by mutations in X-linked MECP2, encoding methyl-CpG-binding protein 2. Nat Genet, 23, 185–8.

Calfa G, Hablitz JJ, Pozzo-Miller L. 2011a. Network hyperexcitability in hippocampal slices from Mecp2 mutant mice revealed by voltage-sensitive dye imaging. J Neurophysiol 105:1768–1784.

Calfa G, Percy AK, Pozzo-Miller L. 2011b. Experimental models of Rett syndrome based on Mecp2 dysfunction. Exp Biol Med (Maywood) 236:3–19.

Cardoza B, Clarke A, Wilcox J, Gibbon F, Smith PE, Archer H, Hryniewiecka-Jaworska A, Kerr M. 2011. Epilepsy in Rett syndrome: Association between phenotype and genotype, and implications for practice. Seizure 20:646–649.

Chang Q, Khare G, Dani V, Nelson S, Jaenisch R. 2006. The disease progression of Mecp2 mutant mice is affected by the level of BDNF expression. Neuron 49:341–348.

Chao HT, Zoghbi HY, Rosenmund C. 2007. MeCP2 controls excitatory synaptic strength by regulating glutamatergic synapse number. Neuron 56:58–65.

Chao HT, Chen H, Samaco RC, Xue M, Chahrour M, Yoo J, Neul JL, Gong S, Lu HC, Heintz N, Ekker M, Rubenstein JL, Noebels JL, Rosenmund C, Zoghbi HY. 2010. Dysfunction in GABA signalling mediates autism-like stereotypies and Rett syndrome phenotypes. Nature 468:263–269.

Chen RZ, Akbarian S, Tudor M, Jaenisch R. 2001. Deficiency of methyl-CpG binding protein-2 in CNS neurons results in a Rett-like phenotype in mice. Nat Genet 27:327–331.

Costa RM, Federov NB, Kogan JH, Murphy GG, Stern J, Ohno M, Kucherlapati R, Jacks T, Silva AJ. 2002. Mechanism for the learning deficits in a mouse model of neurofibromatosis type 1. Nature 415:526–530.

D'Cruz JA, Wu C, Zahid T, El-Hayek Y, Zhang L, Eubanks JH. 2010. Alterations of cortical and hippocampal EEG activity in MeCP2-deficient mice. Neurobiol Dis 38:8–16.

Dani VS, Nelson SB. 2009. Intact long-term potentiation but reduced connectivity between neocortical layer 5 pyramidal neurons in a mouse model of Rett syndrome. J Neurosci 29:11263–11270.

Dani VS, Chang Q, Maffei A, Turrigiano GG, Jaenisch R, Nelson SB. 2005. Reduced cortical activity due to a shift in the balance between excitation and inhibition in a mouse model of Rett syndrome. Proc Natl Acad Sci USA 102:12560–12565.

Di Cristo G. 2007. Development of cortical GABAergic circuits and its implications for neurodevelopmental disorders. Clin Genet 72: 1–8.

Durand S, Patrizi A, Quast KB, Hachigian L, Pavlyuk R, Saxena A, Carninci P, Hensch TK, Fagiolini M. 2012. NMDA receptor regulation prevents regression of visual cortical function in the absence of Mecp2. Neuron 76:1078–1090.

Ehninger D, Li W, Fox K, Stryker MP, Silva AJ. 2008. Reversing neurodevelopmental disorders in adults. Neuron 60:950–960.

Fernandez F, Morishita W, Zuniga E, Nguyen J, Blank M, Malenka RC, Garner CC. 2007. Pharmacotherapy for cognitive impairment in a mouse model of Down syndrome. Nat Neurosci 10:411–413.

Frola E, Patrizi A, Goetz T, Medrihan L, Petrini EM, Barberis A, Wulff P, Wisden W, Sassoe-Pognetto M. 2013. Synaptic competition sculpts the development of GABAergic axo-dendritic but not perisomatic synapses. PLoS One 8:e56311.

Gibson JR, Bartley AF, Hays SA, Huber KM. 2008. Imbalance of neocortical excitation and inhibition and altered UP states reflect network hyperexcitability in the mouse model of fragile X syndrome. J Neurophysiol 100:2615–2626.

Glaze DG, Frost JD Jr, Zoghbi HY, Percy AK. 1987. Rett's syndrome. Correlation of electroencephalographic characteristics with clinical staging. Arch Neurol 44:1053–1056.

Hortnagl H, Tasan RO, Wieselthaler A, Kirchmair E, Sieghart W, Sperk G. 2013. Patterns of mRNA and protein expression for 12 GABAA receptor subunits in the mouse brain. Neuroscience 236: 345–372.

Kleschevnikov AM, Belichenko PV, Villar AJ, Epstein CJ, Malenka RC, Mobley WC. 2004. Hippocampal long-term potentiation suppressed by increased inhibition in the Ts65Dn mouse, a genetic model of Down syndrome. J Neurosci 24:8153–8160.

Kline DD, Ogier M, Kunze DL, Katz DM. 2010. Exogenous brain-derived neurotrophic factor rescues synaptic dysfunction in Mecp2-null mice. J Neurosci 30:5303–5310.

Kohara K, Yasuda H, Huang Y, Adachi N, Sohya K, Tsumoto T. 2007. A local reduction in cortical GABAergic synapses after a loss of endogenous brain-derived neurotrophic factor, as revealed by single-cell gene knock-out method. J Neurosci 27:7234–7244.

Kron M, Howell CJ, Adams IT, Ransbottom M, Christian D, Ogier M, Katz DM. 2012. Brain activity mapping in Mecp2 mutant mice reveals functional deficits in forebrain circuits, including key nodes in the default mode network, that are reversed with ketamine treatment. J Neurosci 32:13860–13872.

Lawrence JJ, McBain CJ. 2003. Interneuron diversity series: Containing the detonation--feedforward inhibition in the CA3 hippocampus. Trends Neurosci 26:631–640.

Li W, Pozzo-Miller L. 2014. BDNF deregulation in Rett syndrome. Neuropharmacology 76 (Part C):737–746.

Li W, Cui Y, Kushner SA, Brown RA, Jentsch JD, Frankland PW, Cannon TD, Silva AJ. 2005. The HMG-CoA reductase inhibitor lovastatin reverses the learning and attention deficits in a mouse model of neurofibromatosis type 1. Curr Biol 15:1961–1967.

Medrihan L, Tantalaki E, Aramuni G, Sargsyan V, Dudanova I, Missler M, Zhang W. 2008. Early defects of GABAergic synapses in the brain stem of a MeCP2 mouse model of Rett syndrome. J Neurophysiol 99:112–121.

Nelson ED, Kavalali ET, Monteggia LM. 2006. MeCP2-dependent transcriptional repression regulates excitatory neurotransmission. Curr Biol 16:710–716.

Nelson ED, Bal M, Kavalali ET, Monteggia LM. 2011. Selective impact of MeCP2 and associated histone deacetylases on the dynamics of evoked excitatory neurotransmission. J Neurophysiol 106:193–201.

Nissenkorn A, Gak E, Vecsler M, Reznik H, Menascu S, Ben Zeev B. 2010. Epilepsy in Rett syndrome—The experience of a National Rett Center. Epilepsia 51:1252–1258.

Noutel J, Hong YK, Leu B, Kang E, Chen C. 2011. Experience-dependent retinogeniculate synapse remodeling is abnormal in MeCP2-deficient mice. Neuron 70:35–42.

Ogier M, Wang H, Hong E, Wang Q, Greenberg ME, Katz DM. 2007. Brain-derived neurotrophic factor expression and respiratory function improve after ampakine treatment in a mouse model of Rett syndrome. J Neurosci 27:10912–10917.

Pelka GJ, Watson CM, Radziewic T, Hayward M, Lahooti H, Christodoulou J, Tam PP. 2006. Mecp2 deficiency is associated with learning and cognitive deficits and altered gene activity in the hippocampal region of mice. Brain 129:887–898.

Pintaudi M, Calevo MG, Vignoli A, Parodi E, Aiello F, Baglietto MG, Hayek Y, Buoni S, Renieri A, Russo S, Cogliati F, Giordano L, Canevini M, Veneselli E. 2010. Epilepsy in Rett syndrome: Clinical and genetic features. Epilepsy Behav 19:296–300.

Preibisch S, Saalfeld S, Tomancak P. 2009. Globally optimal stitching of tiled 3D microscopic image acquisitions. Bioinformatics 25: 1463–1465.

Rubenstein JL, Merzenich MM. 2003. Model of autism: Increased ratio of excitation/inhibition in key neural systems. Genes Brain Behav 2:255–267.

Rueda N, Florez J, Martinez-Cue C. 2008. Chronic pentylenetetrazole but not donepezil treatment rescues spatial cognition in Ts65Dn mice, a model for Down syndrome. Neurosci Lett 433:22–27.

Schmid DA, Yang T, Ogier M, Adams I, Mirakhur Y, Wang Q, Massa SM, Longo FM, Katz DM. 2012. A TrkB small molecule partial agonist rescues TrkB phosphorylation deficits and improves respiratory function in a mouse model of Rett syndrome. J Neurosci 32:1803–1810.

Shahbazian M, Young J, Yuva-Paylor L, Spencer C, Antalffy B, Noebels J, Armstrong D, Paylor R, Zoghbi H. 2002. Mice with truncated MeCP2 recapitulate many Rett syndrome features and display hyperacetylation of histone H3. Neuron 35:243–254.

Shepherd GM, Katz DM. 2011. Synaptic microcircuit dysfunction in genetic models of neurodevelopmental disorders: Focus on Mecp2 and Met. Curr Opin Neurobiol 21:827–833.

Steffenburg U, Hagberg G, Hagberg B. 2001. Epilepsy in a representative series of Rett syndrome. Acta Paediatr 90:34–39.

Szabadics J, Soltesz I. 2009. Functional specificity of mossy fiber innervation of GABAergic cells in the hippocampus. J Neurosci 29:4239–4251.

Vicario-Abejon C, Owens D, McKay R, Segal M. 2002. Role of neurotrophins in central synapse formation and stabilization. Nat Rev Neurosci 3:965–974.

Zhang L, He J, Jugloff DG, Eubanks JH. 2008. The MeCP2-null mouse hippocampus displays altered basal inhibitory rhythms and is prone to hyperexcitability. Hippocampus 18:294–309.

Zhang ZW, Zak JD, Liu H. 2010. MeCP2 is required for normal development of GABAergic circuits in the thalamus. J Neurophysiol 103:2470–2481.

Zhang W, Peterson M, Beyer B, Frankel WN, Zhang ZW. 2014. Loss of MeCP2 from forebrain excitatory neurons leads to cortical hyperexcitation and seizures. J Neurosci 34:2754–2763.